Chapter 12
Charge Drives

Due to the hysteresis exhibited by piezoelectric actuators, many nanopositioning devices require sensor-based closed-loop control. Although closed-loop control can be effective at eliminating nonlinearity at low speeds, the bandwidth compared to open-loop is severely reduced. In addition, sensor-induced noise can significantly degrade the achievable resolution.

In this chapter, charge drives are introduced as a simple alternative when feedback control cannot be applied or provides inadequate performance. These situations arise in high-speed imaging and positioning applications where wide-bandwidth sensor noise is intolerable or where no feedback sensors are present.

12.1 Introduction

Due to their high stiffness, compact size and effectively infinite resolution piezoelectric actuators are universally employed in nanopositioning systems. However, as discussed in Chap. 2 a major disadvantage of piezoelectric actuators is the hysteresis exhibited at high electric fields. To avoid positioning errors, nanopositioning systems require some form of compensation for piezoelectric nonlinearity. Techniques to accomplish this including feedback and feedforward control were reviewed in Chap. 1.

Since the late 80s, it has been known that driving piezoelectric transducers with current or charge rather than voltage significantly reduces hysteresis (Newcomb and Flinn 1982). Simply by regulating the current or charge, a 5-fold reduction in the hysteresis can be achieved (Ge and Jouaneh 1996; Fleming 2010). Although the circuit topology of a charge or current drive is much the same as a simple voltage amplifier, the uncontrolled nature of the output voltage typically results in the load capacitor being linearly charged. Recent developments have eliminated low-frequency drift and permitted grounded loads, which are necessary in nanopositioning systems (Fleming and Moheimani 2006; Fleming and Leang 2008; Fleming 2013).

A. J. Fleming and K. K. Leang, *Design, Modeling and Control of Nanopositioning Systems*, Advances in Industrial Control,
DOI: 10.1007/978-3-319-06617-2_12,

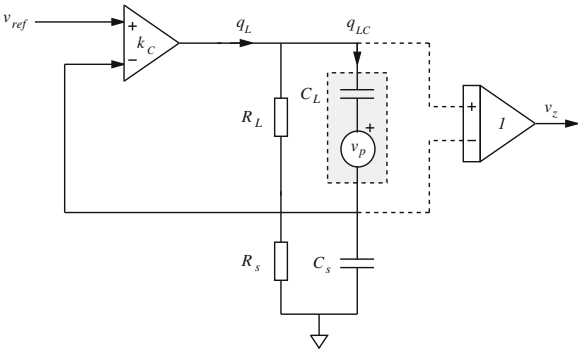

Fig. 12.1 Simplified diagram of a generic charge source

In the following section, the design of charge drives is discussed. These are then applied to both stack actuators and piezoelectric tube actuators in Sects. 12.3 and 12.4, respectively. Section 12.5 contains information specific to the implementation of charge drives for multielectrode piezoelectric tube nanopositioners, which are commonly used in microscopy applications. A summary of the advantages and drawbacks of charge drives then follows in Sects. 12.6 and 12.7.

12.2 Charge Drives

The simplified schematic of a charge drive circuit is shown in Fig. 12.1. The piezoelectric load, modeled as a capacitor and voltage source v_p, is shown in gray. The high gain feedback loop (k_C) works to equate the applied reference voltage v_{ref}, to the voltage across a sensing capacitor C_s. Neglecting the resistances R_L and R_s, at frequencies well within the bandwidth of the control loop, the load charge q_L is equal to

$$q_L = V_{\text{ref}} C_s, \tag{12.1}$$

i.e., we have a charge amplifier with a gain of C_s Coulombs/V.

The foremost difficulties associated with the charge drive in Fig. 12.1 are due to the resistances R_L and R_s. These resistances model the parasitic leakage resulting from the input terminals of the feedback opamps, capacitor dielectric leakage, and v_z measurement. In practice, this parasitic resistance is often swamped with additional physical resistances required to manage the voltage drift associated with the input bias current of the feedback network and instrumentation.

If there exists a parallel load resistance R_L, the actual charge $q_{LC}(s)$ flowing through the load transducer becomes

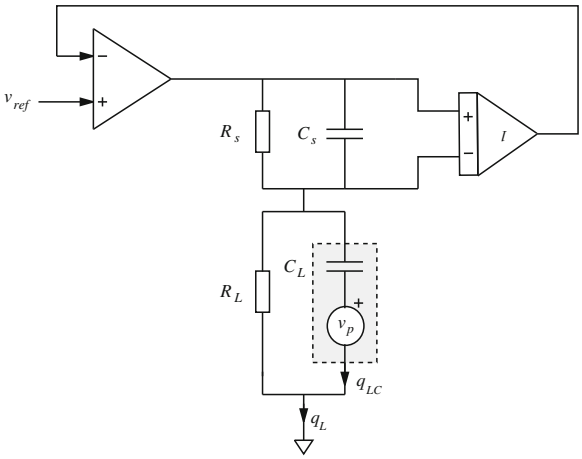

Fig. 12.2 DC accurate charge source for grounded capacitive loads (Fleming and Moheimani 2006). The piezoelectric load, modeled as a capacitor and voltage source v_p, is shown in gray

$$q_{LC}(s) = q_L(s)\frac{s}{s + \frac{1}{R_L C_L}}. \tag{12.2}$$

The amplifier now contains a high-pass filter with cutoff $\omega_c = \frac{1}{R_L C_L}$. That is,

$$\frac{q_{LC}(s)}{V_{\text{ref}}(s)} = C_s \frac{s}{s + \frac{1}{R_L C_L}}. \tag{12.3}$$

In a typical piezoelectric tube drive scenario, with C_L=10 nF, a 1 μA output offset current requires a 10 MΩ parallel resistance to limit the DC voltage offset to 10 V. Phase lead exceeds 5° below 18 Hz. Such poor low-frequency performance precludes the use of charge drives in applications requiring accurate low-frequency tracking, e.g., Atomic Force Microscopy.

A solution for the problem of voltage drift was first presented in Fleming and Moheimani (2004). An auxiliary voltage feedback loop was included to correct low-frequency behavior and allow for constant charge offsets. The circuit implementation required the design of separate voltage and charge feedback controllers. A simplified design relying on the intrinsic voltage control offered by the parasitic resistances was later presented in Yi and Veillette (2005). Neither of these circuits were capable of driving grounded loads. As piezoelectric tubes have multiple external electrodes and a common (often grounded) internal electrode, the requirement for a grounded-load is a necessity.

A charge-driven circuit designed for nanopositioning systems with grounded loads was presented in Fleming and Moheimani (2006). This circuit is shown in Fig. 12.2. The piezoelectric load, modeled as a capacitor and voltage source v_p, is shown

in gray. The amplifier uses a high-voltage differential buffer to equate the voltage measured across the sensing capacitor C_s to the reference voltage v_{ref}.

Neglecting the resistances R_L and R_s, at frequencies well within the bandwidth of the control loop, the load charge q_L is equal to

$$q_L = V_{\text{ref}} C_s. \tag{12.4}$$

That is, the gain is C_s Coulombs/V. When connected to a capacitive load, the equivalent voltage gain is C_s/C_L.

To understand the operation of the amplifier at low frequencies, the transfer function from the applied reference voltage v_{ref} to the load charge q_{LC} must be studied. This can be obtained by first considering the transfer function between the applied reference voltage v_{ref} and the charge q_L,

$$\frac{q_L(s)}{v_{\text{ref}}(s)} = C_s \frac{s + \frac{1}{C_s R_s}}{s}. \tag{12.5}$$

The transfer function from the reference voltage to load charge can then be found by combining Eqs. (12.5) and (12.2)

$$\begin{aligned} \frac{q_{LC}(s)}{v_{\text{ref}}(s)} &= \frac{q_L(s)}{v_{\text{ref}}(s)} \frac{q_{LC}(s)}{q_L(s)} \\ &= C_s \frac{s + \frac{1}{C_s R_s}}{s} \frac{s}{s + \frac{1}{R_L C_L}} \end{aligned} \tag{12.6}$$

That is, the transfer function contains a pole due to the load resistance R_L and a zero due to the sensing resistance R_s. These dynamics can be eliminated by setting $C_L R_L = C_s R_s$, i.e.,

$$\frac{R_L}{R_s} = \frac{C_s}{C_L}. \tag{12.7}$$

Now the amplifier has no low-frequency dynamics and a constant gain of C_s Coulombs/Volt. Effectively the two resistances R_L and R_s form a voltage amplifier at low frequencies that has the same gain as the charge drive at higher frequencies.

As the amplifier can be viewed as the concatenation of a voltage and charge amplifier, it is important to identify the frequency range where each mode of operation is dominant. Consider the schematic shown in Fig. 12.3. If v_{ref} is set to zero, during perfect charge operation i.e., when q_{LC} is correctly regulated to zero, the voltage v_z will be equal to v_p. During voltage dominant behavior, v_z will be regulated to zero. Such characteristics can easily be measured experimentally.

When $v_{\text{ref}} = 0$, which implies $q_L = 0$ the transfer function from v_p to v_z reveals the voltage or charge dominance of the amplifier. At frequencies where $v_z \approx v_p$, the amplifier is charge dominant, and voltage dominant when $v_z \approx 0$. For the hybrid amplifier shown in Fig. 12.2, when $v_{\text{ref}} = 0$,

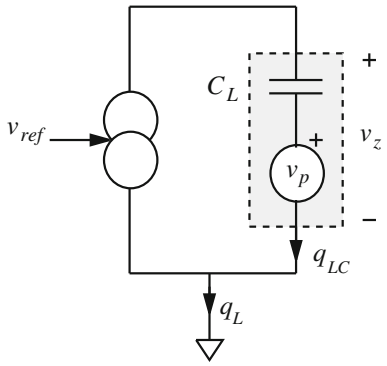

Fig. 12.3 Test for voltage/charge dominance

$$\frac{v_z(s)}{v_p(s)} = \frac{s}{s + \frac{1}{R_L C_L}}. \tag{12.8}$$

That is, at frequencies above $\frac{1}{R_L C_L}$ s^{-1} the amplifier is charge dominant, and voltage dominant below. Obviously, given Eq. (12.8), the objective will be to select a load resistor R_L as large as possible. This may be limited by other factors such as opamp current noise attenuation, bias-current induced offset voltages, and the common-mode and differential leakage of the opamp. In practice $\frac{v_z(s)}{v_p(s)}$ is best measured by simply applying a voltage to another electrode and using that as a reference, as the frequencies under consideration are well below the tube's first mechanical resonance, the applied voltage will be related by a constant. Such experiments are described in Sect. 6.4.2

Alike a typical voltage amplifier, the hybrid amplifier offers little or no hysteresis reduction over the frequency range of voltage dominance. For the same reason, no improvement in creep can be expected. Creep time-constants are usually greater than 10 min, which in this discussion, is effectively DC. At these frequencies, the amplifier behaves analogously to a standard voltage amplifier.

The high frequency bandwidth of a charge drive is limited by the same factors as a voltage amplifier. Bandwidth is limited by a secondary pole in the feedback loop formed by the output impedance and load capacitance. Due to additional phase lag contributed by this secondary pole, the amplifiers bandwidth is restricted to around one-tenth the pole's frequency if large stability margins are to be retained.

In addition to the secondary pole discussed above, charge drives are also limited by the bandwidth of the differential amplifier in the charge measuring circuit. If this is near or less than the frequency of the secondary pole, it will degrade phase margin and necessitate a reduction in bandwidth. Although high voltage differential amplifiers such as the AD629 are available for a few dollars, discrete designs can achieve much higher bandwidths, but with increased complexity. If closed-loop bandwidths of greater than a 100 Hz are required, a high-performance differential amplifier is mandatory.

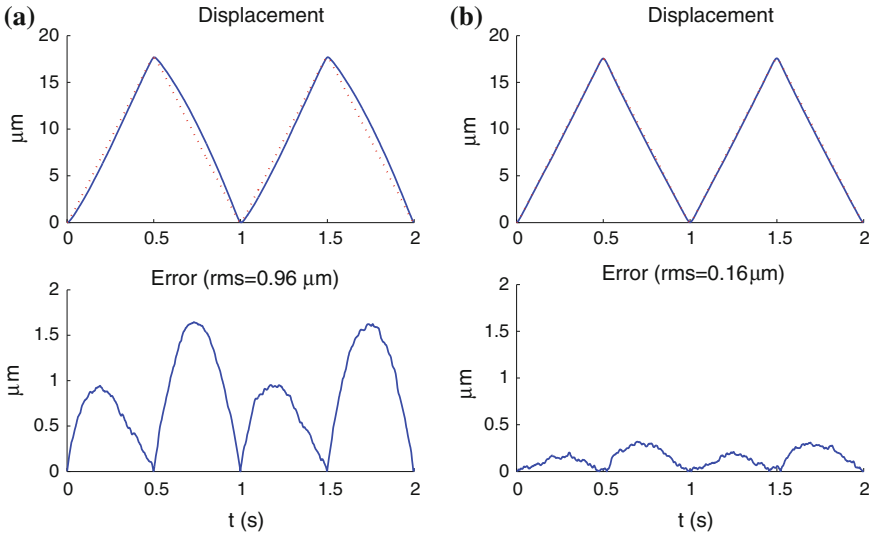

Fig. 12.4 The displacement of the P733 nanopositioner driven by a voltage amplifier (**a**) and charge drive (**b**). The *dotted line* in the displacement plot is the input signal scaled to act as a reference

12.3 Application to Piezoelectric Stack Nanopositioners

In this section, the positioning performance of a charge drive is compared to a voltage amplifier when driving the Physik Instrumente P733 nanopositioner described in Sect. 3.2.2. This device has a specified range of $30 \times 30 \times 10\,\mu$m in the X, Y, and Z axis.

In this experiment, the charge drive is connected to the Z-axis actuator, which has a capacitance of 3.2 μF. To provide a voltage gain 20, equal to that of the voltage amplifier, the charge gain is set to 64 μC/V.

In Fig. 12.4, the full-range displacement of the nanopositioner is plotted in response to a 1 Hz triangle wave with both voltage and charge actuation. With voltage drive, the maximum absolute positioning error is 1.6 μm, or 9.3 % of the range. In Fig. 12.4b, the use of a charge drive reduces the maximum positioning error to only 300 nm, or 1.8 % of the range, which may be a tolerable error in many applications.

The hysteresis exhibited by the actuator is most clearly observed by plotting the reference command against displacement. This is performed for both voltage and charge actuation in Fig. 12.5. Clearly, the charge drive significantly reduces the maximum deviation from linear. When plotting hysteresis it is important to ensure that no other sources of phase delay are present in the data. This includes linear phase lag due to mechanical dynamics, amplifiers, sensors, and other instruments in the signal chain. As such effects can be erroneously neglected, linear phase lag can be mistaken for hysteresis since it results in a similar waveform. The most common source of phase lag is from driving amplifiers, which are typically low in bandwidth

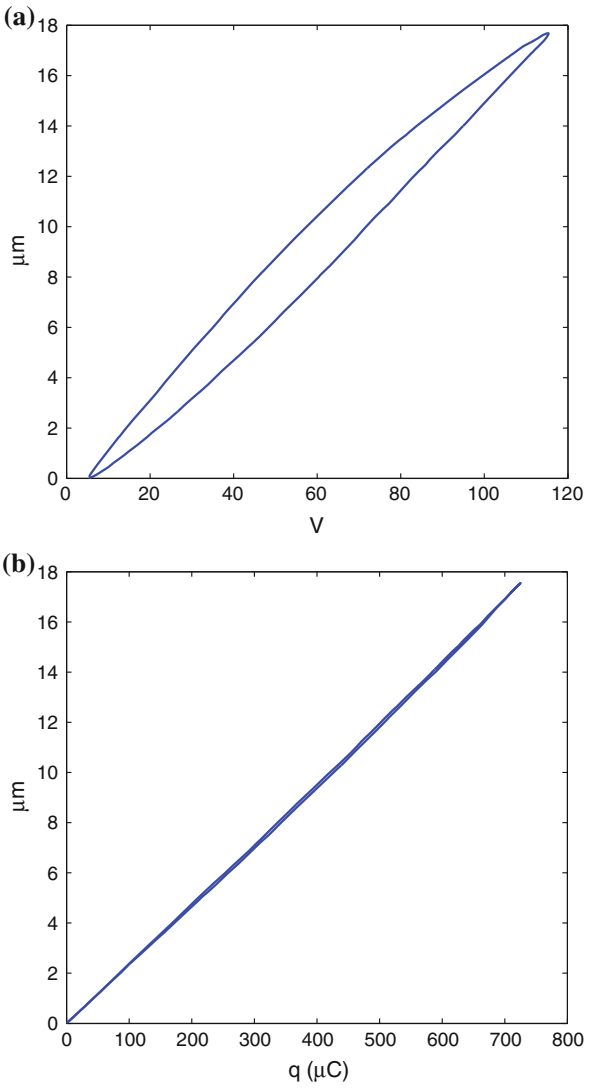

Fig. 12.5 The displacement of the P-733 nanopositioner as a function of voltage (**a**) and charge (**b**). The input was a 1 Hz triangle wave

when driving large capacitive loads. In these experiments, the driving frequency of 1 Hz is at least two decades lower than the bandwidth of amplifiers, sensors, and mechanical dynamics, thus additional sources of phase lag are negligible.

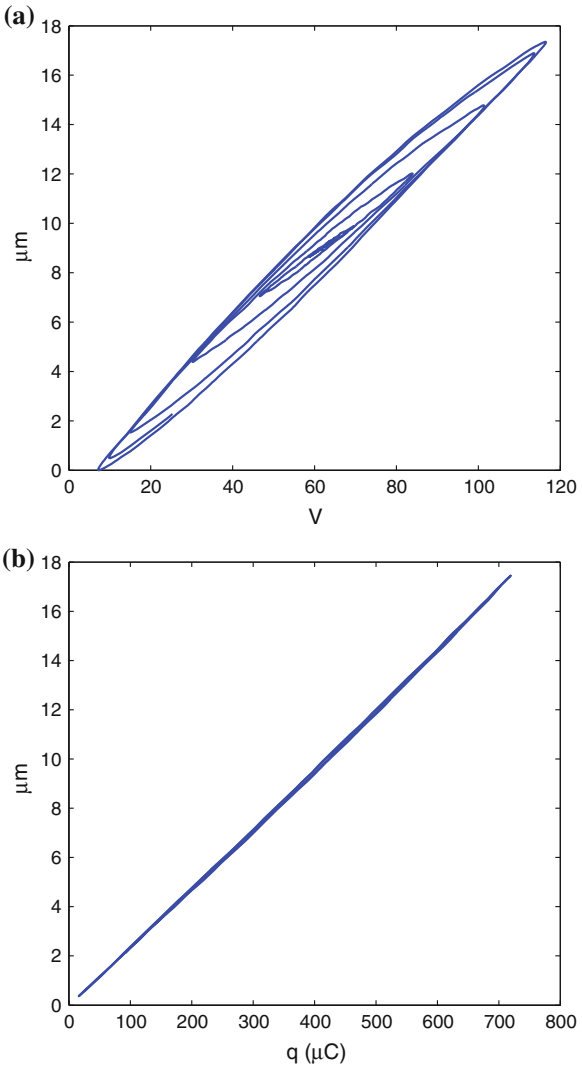

Fig. 12.6 The displacement of the P733 nanopositioner as a function of voltage (**a**) and charge (**b**). The input was a 1 Hz triangle wave, ramped in amplitude over 5 s

In addition to the worst-case, or full range hysteresis, it is also useful to observe the dependence on driving amplitude. In Fig. 12.6, the displacement of the nanopositioner is plotted in response to a 1 Hz triangle wave that is increase in amplitude over five periods. While the voltage-driven positioning nonlinearity markedly increases with signal amplitude, the charge-driven nonlinearity remains low in all cases.

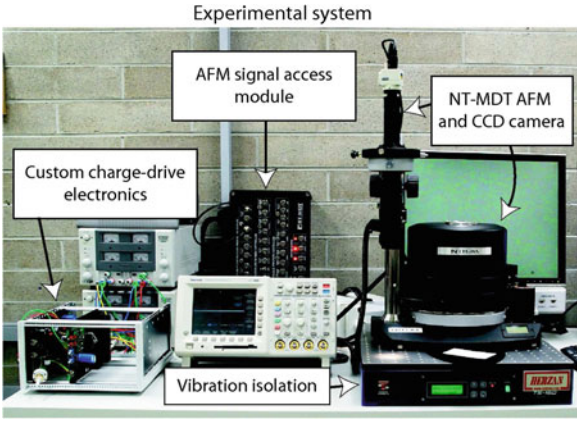

Fig. 12.7 A photograph of the experimental SPM system with charge drive electronics

12.4 Application to Piezoelectric Tube Nanopositioners

A key component of Scanning Probe Microscopes (SPM's) (Meyer et al. 2004) is the nanopositioning system required to manoeuvre the probe or sample. To avoid imaging artefacts, SPMs require some form of compensation for the positioning nonlinearity. Techniques to accomplish this, including feedback, feedforward and image-based compensation are reviewed in Abramovitch et al. (2007) and Clayton et al. (2009).

The most popular technique for compensation in commercial scanning probe microscopes is sensor-based feedback control using integral or Proportional-Integral (PI) control. Such controllers are simple, robust to modeling error, and due to high loop-gain at low-frequencies, effectively reduce piezoelectric nonlinearity. However, the disadvantages of closed-loop control include: cost, additional complexity, limited bandwidth, and sensor-induced noise.

In this section, charge control is applied to linearize an SPM positioning stage. The aim is to provide a simple alternative to feedback control where such techniques cannot be applied or provide inadequate performance. For example, in high-speed imaging (Ando et al. 2005; Humphris et al. 2005; Rost et al. 2005; Fantner et al. 2006; Picco et al. 2007; Fleming 2009), it is difficult or impossible to achieve a satisfactory controller bandwidth. Sensor noise is another major issue when atomic resolution is required, particularly if the controller bandwidth is greater than a few Hertz. Also, in many 'home-made' and application specific microscopes, feedback sensors are not present and the only control option is open-loop, which is the case for all of the scanners reported in Ando et al. (2005), Humphris et al. (2005), Rost et al. (2005), Fantner et al. (2006), Picco et al. (2007) and Fleming (2009).

Pictured in Fig. 12.7, an NT-MDT Ntegra SPM was retrofitted with a charge drive on the fast scanning x-axis. A signal access module allowed direct access to the

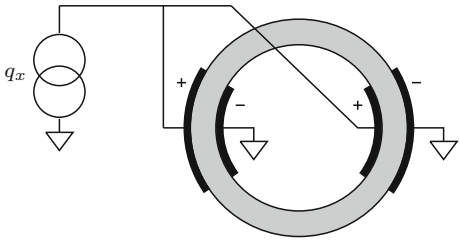

Fig. 12.8 *Top view* of the tube scanner. The x-axis electrodes are quartered on the inside and outside and driven in parallel by the charge source

scanner electrodes and reference signal. The charge gain was set to provide an equivalent voltage gain equal to the standard internal controller gain of 15. Accordingly, no modifications to the scan-controller or software interface were required.

The scanner is an NT-MDT Z50309cl piezoelectric tube scanner with 100 μm range. As shown in Fig. 12.8, the tube has quartered internal and external electrodes that allow the scanner to be driven in a bridged configuration. That is, where the internal and external electrodes are driven with equal but opposite voltages. The naming arises from the way in which the electrodes 'bridge' the two driving sources together, effectively doubling the differential voltage experienced by the actuator. Compared to the more popular grounded internal electrode configuration, the bridged configuration requires half the driving voltage to achieve full range. In these experiments, one pair of electrodes are grounded to allow an analogy with stack-based positioners that are driven with this configuration. Further discussion specific to piezoelectric tube scanners, including the application of charge drives to bridged electrodes, is contained in Sect. 12.5.

During imaging, the AFM was operated in constant height, contact mode, using a cantilever with spring constant 0.2 N/m. The lateral deflection of the piezo actuator was measured using capacitive sensors incorporated into the scanner assembly. A 1 Hz triangle wave was applied to develop scans of 5, 20, and 50 μm, corresponding to 5, 20, and 50 % of the maximum scan range. The scanner trajectories and tracking errors are plotted in Fig. 12.9. Maximum absolute error for voltage and charge drive is compared in Table 12.1.

The displacement nonlinearity was only 2 % in the 5 μm voltage-driven scan; this was reduced to 0.86 % using charge actuation. In the 20 and 50 μm scans, voltage-driven nonlinearity was more significant, 4.9 and 7.2 %, respectively. This was reduced to 0.36 and 0.78 % using charge, a reduction of 93 and 89 %.

AFM images of a 20 nm feature-height parallel calibration grating (3 μm pitch) are pictured in Fig. 12.10. Images were recorded by linearizing the y-axis with a capacitive sensor and driving the x-axis with voltage, then charge. For the 5 μm scan in Fig. 12.10a, the 2 % voltage nonlinearity is not discernable. However, for the 20 and 50 μm scans in Fig. 12.10c, e, the 4.9 and 7.2 % nonlinearity clearly distorts the image. In all three charge-driven scans, Fig. 12.10b–f, the nonlinearity is less than 1 % and image distortion is imperceptible. Reference lines in Fig. 12.10 are superimposed on each image for comparision.

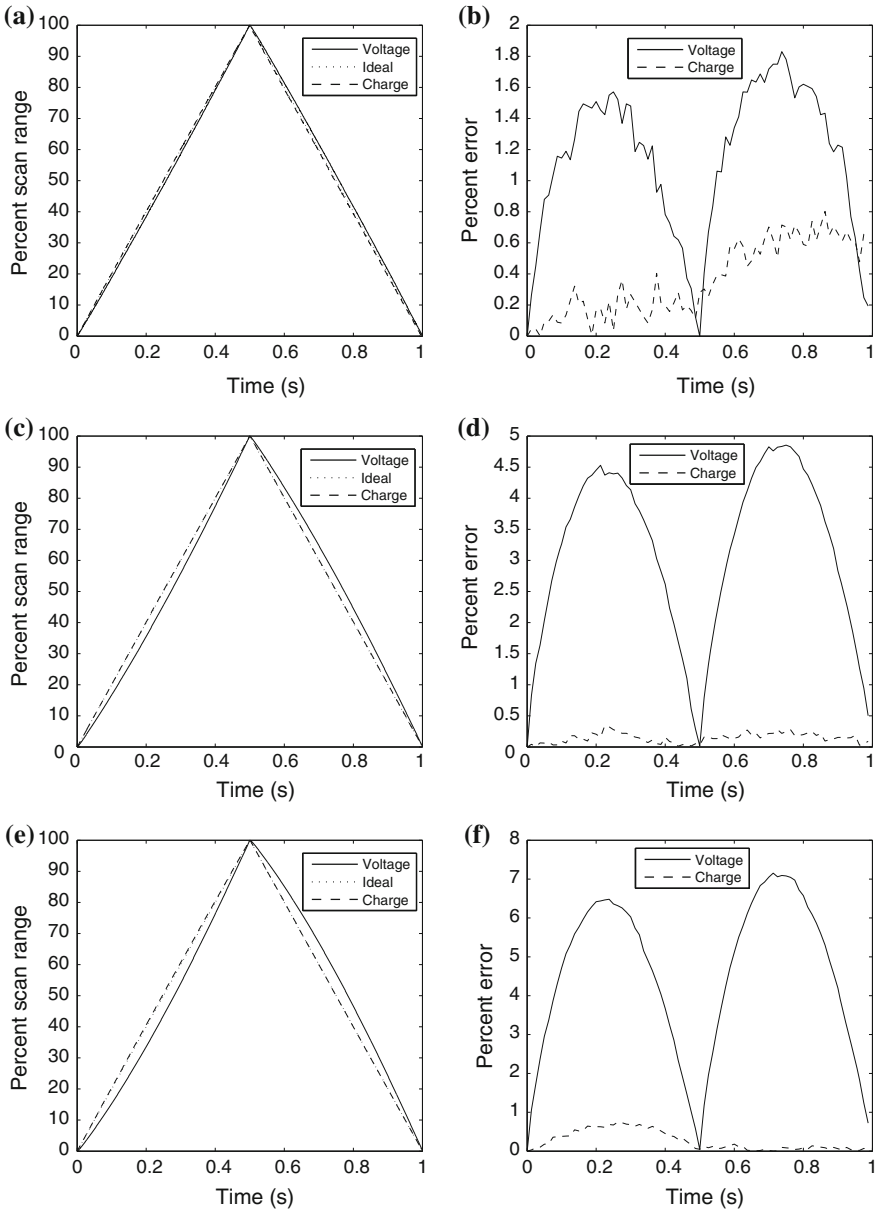

Fig. 12.9 The measured scanner deflection and percentage error for 5, 20, and 50 μm scans. The input was a 1 Hz triangle wave. **a** 5 μm scan. **b** 5 μm scan error. **c** 20 μm scan. **d** 20 μm scan error. **e** 50 μm scan. **f** 50 μm scan error

Table 12.1 Open-loop scan error with voltage and charge actuation

Scan range (μm)	Absolute Scan Error		Reduction (%)
	Voltage (%)	Charge (%)	
5	2.0	0.86	54
20	4.9	0.36	93
50	7.2	0.78	89

12.5 Alternative Electrode Configurations

Commercial scanning probe microscopes contain piezoelectric tube nanopositioners that utilize one of two possible electrode configurations: the grounded internal electrode configuration, or quartered internal electrode configuration. The application of charge drives to each of these scenarios is discussed below.

The techniques discussed in this section are not relevant to piezoelectric stack-based scanners. These actuators are unipolar and require only a single voltage or charge source with one grounded electrode. This configuration is used in the previous sections.

12.5.1 Grounded Internal Electrode

The most common electrode configuration on piezoelectric tube scanners is a single-grounded internal electrode with quartered external electrodes. Electrodes on opposite sides are driven with equal but opposite voltages to induce deflection in that axis. Although the tubes themselves are simple to fabricate, this configuration requires two bipolar voltage amplifiers for each electrode, four in total to achieve x and y lateral motion.

As charge amplifiers are more complicated than voltage amplifiers it is undesirable to require four of them. However, the drive requirements can be simplified if the two electrodes are mechanically and electrically identical. If so, the voltage induced on the charge driven electrode can simply be negated and applied to the opposite electrode as shown in Fig. 12.11a. For an explanation, consider the electrical equivalent circuit in Fig. 12.11b. The piezoelectric elements under each left- and right-hand electrode are modeled as the capacitances c_{p1} and c_{p2} in series with the piezoelectric strain voltages v_{p1} and v_{p2}. As the electrodes are on opposite sides of the tube, and equal but opposite voltages are applied to both electrodes, the piezoelectric strain voltages v_{p1} and v_{p2} will also be equal but opposite. Under this assumption, if the voltage v_1 is applied oppositely to the right-hand electrode, i.e., if $v_2 = -v_1$, the charge q_2 will be equal but opposite to q_1, and the tube will behave linearly as if two independent charge amplifiers were used.

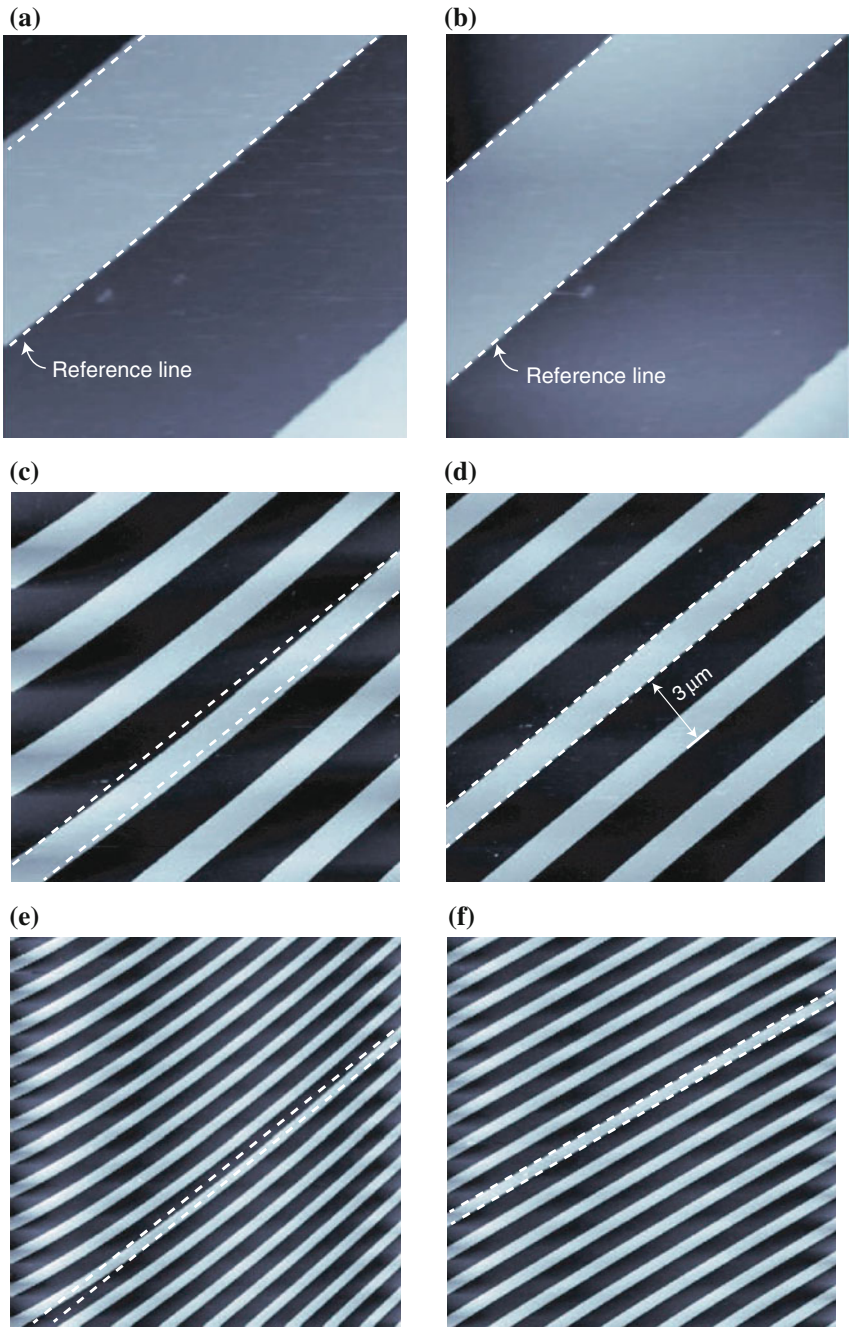

Fig. 12.10 A comparison of images recorded using voltage and charge actuation. The sample is a periodic calibration grating with 20 nm feature height. **a** Voltage drive 5 × 5 µm. **b** Charge drive 5 × 5 µm. **c** Voltage drive 20 × 20 µm. **d** Charge drive 20 × 20 µm. **e** Voltage drive 50 × 50 µm. **f** Charge drive 50 × 50 µm.

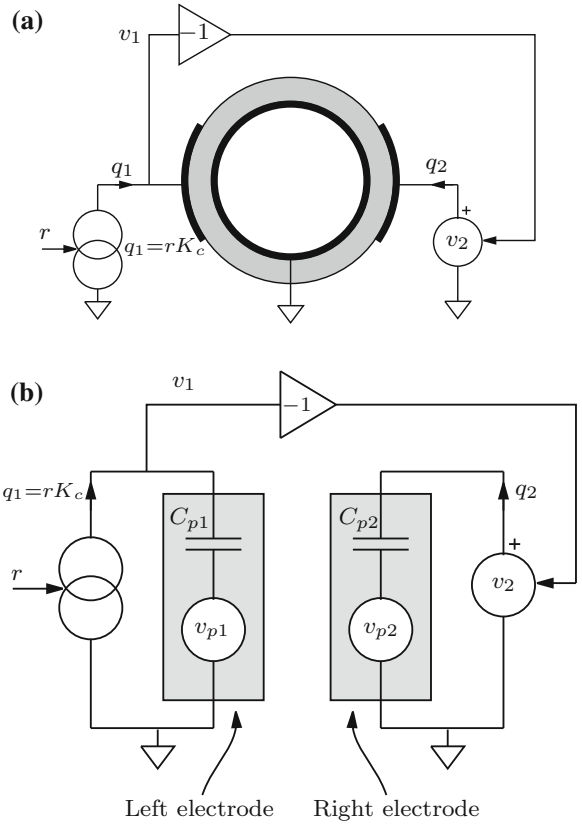

Fig. 12.11 The grounded internal electrode configuration (*top*) and eqivalent electrical circuit (*bottom*)

12.5.2 Quartered Internal Electrode

As illustrated in Fig. 12.8 and discussed in Sect. 12.4, the quartered internal electrode configuration, although more difficult to fabricate, requires half the voltage of the previous technique to achieve the same deflection. This is a major advantage as high-voltage amplifiers are costly and two independent amplifiers are required for each axis.

The application of a charge drive to bridged electrodes is somewhat different from the standard voltage-driven configuration. Usually opposite voltages are applied to the inner and outer electrode while the left- and right-hand electrode pairs are connected in parallel. As the bridged electrodes connect the two sources in series, two charge drives would not form a stable circuit. This is analogous to connecting two voltage sources in parallel.

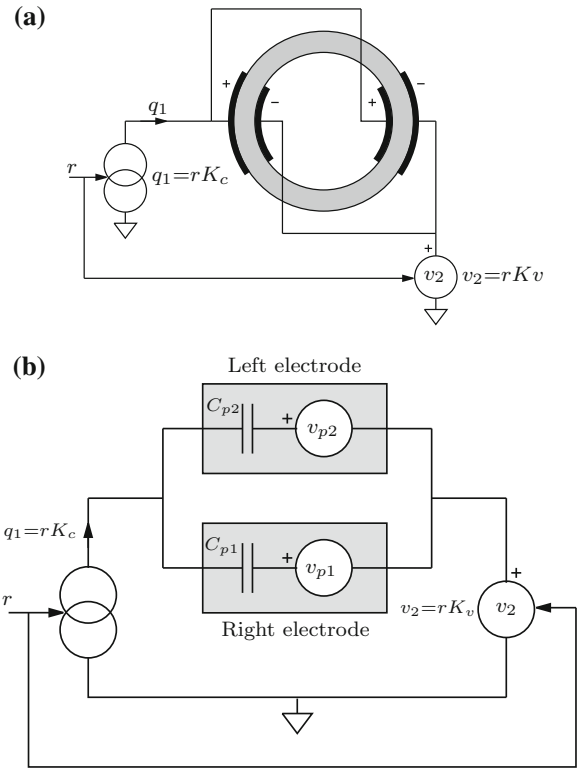

Fig. 12.12 The quartered, or bridged internal electrode configuration (*top*) and eqivalent electrical circuit (*bottom*)

A suitable electrical connection that requires only a single charge drive is shown in Fig. 12.12. Interestingly, varying the voltage on the electrodes marked negative does not alter the amount of deposited charge or corresponding displacement. However, by setting the voltage on the negative electrode approximately equal but opposite to the voltage developed by the charge drive, twice as much charge can be deposited with the same voltage. So far as the charge drive is concerned, driving the negative electrodes with an opposite voltage results in a doubling of the load capacitance. Thus, twice as much charge can be deposited with the same voltage.

The electrical equivalent circuit of a charge-driven tube with internal electrodes is contained in Fig. 12.12b. If a reference signal r is applied to a charge amplifier with gain K_c Coulombs/Volt, the load voltage will be approximately

$$v_1 = rK_c/C_p \tag{12.9}$$

(neglecting v_{p1} and v_{p2} that are much lesser than $v_1 - v_2$), where C_p is the parallel combination of C_{p1} and C_{p2}. Thus, if the voltage gain K_v is set to $K_v = -K_c/C_p$,

the voltage v_2 will be approximately $-v_1$ and the charge drive will result in an approximately balanced voltage across the load. Another option is to adopt a similar approach to the previous section, however this requires additional circuitry to buffer and measure the voltage developed by the charge drive (v_1).

The configuration in Fig. 12.12a was implemented on the experimental setup discussed in Sect. 12.4. The bridged load allowed a 200 V charge drive to obtain the full 400 V differential required for maximum deflection. An experimental 100 μm scan comparing both voltage and charge actuation is plotted in Fig. 12.13. At full range, the maximum scan error using voltage is 9.7 %, compared to 2.0 % using charge.

It is interesting to note the assymetry of nonlinearity in Figs. 12.9 and 12.13. The decreasing part of the charge-driven scan has less nonlinearity in all cases. The maximum charge-driven scan error, even at full range with bridged electrodes is only 0.5 % compared to 9.7 % using voltage.

12.6 Charge Versus Voltage

In this section, the advantages and drawbacks of charge drives are discussed for open-loop positioning applications.

12.6.1 Advantages

There are two motivating factors for the use of charge drives in nanopositioning systems: reduction of hysteresis; and vibration compensation.

In Sect. 12.4, the nonlinearity of a tube scanner driven to half its full-scale range was measured at 7.2 %. Subsequent images demonstrate that this magnitude of error is intolerable. Conversely, when driven with charge, scan error remains below 1 % and is imperceptible in the images. Thus, while closed-loop control of voltage-driven nanopositioners is mandatory in imaging applications, the use of charge drives can provide satisfactory linearity with no feedback. Follow-on benefits include zero sensor-induced noise, no controller imposed bandwidth limitations, simpler scanner design (due to the absence of sensors) and lower cost.

In high-speed nanopositioning and microscopy applications (Ando et al. 2005; Humphris et al. 2005; Rost et al. 2005; Fantner et al. 2006; Picco et al. 2007; Fleming 2009) where feedback control is not feasible, the use of charge drives has the potential to significantly increase imaging performance. Feedback control is not an option due to bandwidth and noise considerations.

In addition to hysteresis reduction, damping of resonant modes can also be accomplished without the need for feedback. In Chap. 6, the first mechanical scanner resonance is attenuated by shunting the actuator electrodes with a parallel passive

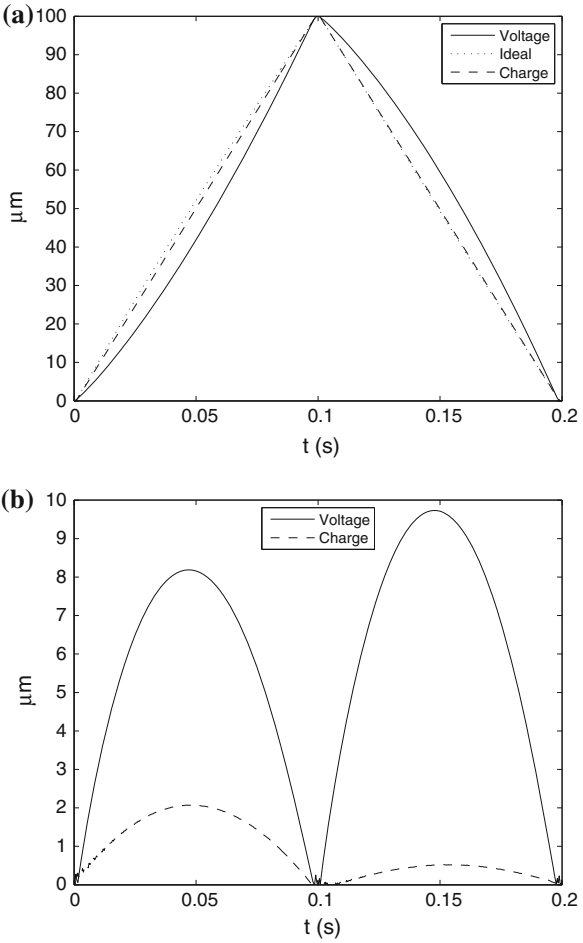

Fig. 12.13 The bridged voltage and charge-driven deflection in response to a 5 Hz triangle wave (**a**); and scan error (**b**)

impedance. The impedance is tuned to resonate with the transducers capacitance at the frequency of problematic modes. Greater than 20 dB attenuation of the first lateral mode is demonstrated.

12.6.2 Disadvantages

The disadvantages of charge drives are the increased circuit complexity, voltage range reduction and necessity for gain tuning.

Although floating-load charge drives are similar to standard inverting voltage amplifiers, the grounded-load configuration in Fig. 12.2 requires a high-performance differential buffer. The differential buffer requires high-input impedance, common-mode-range equal to the high-voltage supply and common-mode-rejection-ratio greater than 80 dB over the bandwidth of the amplifier. These specifications are not met by available integrated devices but can be achieved with discrete designs, with increased circuit complexity. However, if the application does not require operation beyond 100 Hz, the differential buffer can be constructed easily with off-the-shelf parts, for example the AD629.

The differential buffer present in the grounded-load configuration contributes some additional noise, which is likely to be greater than the thermal noise of resistors in a voltage feedback amplifier. Thus, a grounded-load charge drive will generate more noise than a voltage amplifier of the same gain. The situation is different for a floating-load charge drive. This does not require a differential buffer and can provide less noise than a comparable voltage amplifier as the feedback network does not contribute thermal noise.

In addition to amplifier noise, electromagnetic interference can contribute strongly to circuits with high-impedance nodes. In this regard, the grounded-load configuration is superior to the floating-load configuration as it is more easily shielded.

Another consideration is the reduction in voltage range due to the drop across the sensing capacitor C_s. The output voltage range is limited by the maximum amplifier voltage minus the feedback voltage. This requires a slightly higher supply voltage to develop the same transducer displacement. For high-voltage devices greater than 100 V, the maximum 10 V drop across C_s is not significant. However, in lower voltage applications, this reduction may become significant as standard ICs are limited to between 36 and 50 V. Simply increasing C_s and decreasing V_{ref} is an option for improving voltage range.

Aside from issues with the actual circuitry, the only significant difference between voltage and charge actuation is the need to adjust charge gain. At DC and low-frequencies, the voltage gain is fixed by the ratio of resistances R_L and R_s—these are easily interchanged or adjusted. To achieve the same gain at higher frequencies, C_s would need to be adjusted accordingly. This is impossible as variable capacitors of sufficient capacitance are not available. A better option is to select C_s larger than necessary, then add a gain α to the differential buffer, this allows a reduction of charge gain to that desired. After the charge gain is set, the resistance ratio R_L/R_s needs to be adjusted to $\alpha C_s/C_L$.

12.7 Impact on Closed-Loop Control

At normal imaging speeds of less than 10 Hz scan-rate, simple integral controllers with either damping controllers or notch filters for resonance compensation provide sufficient performance and are widely applied (Leang and Devasia 2007). Over the frequency range where loop-gain is greater than 1, typically from DC to tens of Hz, the

scanner displacement tracks additive sensor noise. Even with low-noise capacitive sensors (noise density 20 pm/$\sqrt{\text{Hz}}$), a controller bandwidth of 100 Hz results in greater than 1 nm peak-peak noise. This precludes standard closed-loop scanners from achieving atomic resolution. The situation can be improved by dropping the controller bandwidth to 10 Hz. Although this provides the possibility for atomic resolution, the limited bandwidth restricts usage to extremely slow scanning only.

With charge control, sensors are not required for linearization. Thus, no sensor-induced noise is present. However, to eliminate creep and thermal drift in the scanner, a slow feedback loop can be added. In this case, sensor noise is negligible as the bandwidth of such a control-loop would be less than 1 Hz.

Charge drives are also suited to systems containing feedforward controllers. Many linear feedforward controllers have been proposed that significantly improve the speed and accuracy of positioning stages with little added complexity, a review of such techniques can be found in Abramovitch et al. (2007), Leang et al. (2009) and Clayton et al. (2009). In the past, a major drawback of feedforward control has been the difficulty of eliminating hysteresis over a wide variety of operating conditions. When using charge drives, hysteresis is heavily reduced and feedforward control can be effectively applied, even at high scan ranges Clayton et al. (2008).

12.8 Chapter Summary

In this chapter, charge drives were introduced as an open-loop technique for reducing the hysteresis exhibited by piezoelectric actuators. Experimental results demonstrated an improvement in linearity of greater than 90 % for both piezoelectric tube and stack actuated nanopositioning systems. The advantages are:

- Reduction of hysteresis to less than 1 % of the scan range.
- Straightforward replacement for voltage amplifiers.
- Compatible with sensor-less vibration control.

Disadvantages include:

- Greater circuit complexity.
- Requires tuning to set the gain.
- Low frequency performance is limited by the transducer capacitance.

References

Abramovitch DY, Andersson SB, Pao LY, Schitter G (2007) A tutorial on the mechanisms, dynamics, and control of atomic force microscopes. In: Proceedings of American Control Conference, New York City, NY, Jul 2007, pp 3488–3502

Ando T, Kodera N, Uchihashi T, Miyagi A, Nakakita R, Yamashita H, Matada K (2005) High-speed atomic force microscopy for capturing dynamic behavior of protein molecules at work.e-J Surf Sci Nanotechnol 3:384–392

Clayton GM, Tien S, Devasia S, Fleming AJ, Moheimani SOR (2008) Inverse-feedforward of charge controlled piezopositioners. Mechatronics 18:273–281

Clayton GM, Tien S, Leang KK, Zou Q, Devasia S (2009) A review of feedforward control approaches in nanopositioning for high-speed SPM. J Dyn Syst Meas Contr 131(1–19):61–101

Fantner GE, Schitter G, Kindt JH, Ivanov T, Ivanova K, Patel R, Holten-Andersen N, Adams J, Thurner PJ, Rangelow IW, Hansma PK (2006) Components for high speed atomic force microscopy. Ultramicroscopy 106(2–3):881–887

Fleming AJ (2009) High-speed vertical positioning for contact-mode atomic force microscopy. In: Proceedings of IEEE/ASME international conference on advanced intelligent mechatronics, Singapore, July 2009, pp. 522–527

Fleming AJ (2010) Quantitative SPM topographies by charge linearization of the vertical actuator. Rev Sci Instrum 81(10):103701–103705

Fleming AJ (2013) Charge drive with active DC stabilization for linearization of piezoelectric hysteresis. IEEE Trans Ultrason Ferroelectr Freq Control 60(8):1630–1637 (published: 01)

Fleming AJ, Leang KK (2008) Charge drives for scanning probe microscope positioning stages. Ultramicroscopy 108(12):1551–1557

Fleming AJ, Moheimani SOR (2004) Hybrid DC accurate charge amplifier for linear piezoelectric positioning. In: Proceedings 3rd IFAC symposium on mechatronic systems, Sydney, Australia, Sept 2004

Fleming AJ, Moheimani SOR (2006) Sensorless vibration suppression and scan compensation for piezoelectric tube nanopositioners. IEEE Trans Control Syst Technol 14(1):33–44

Ge P, Jouaneh M (1996) Tracking control of a piezoceramic actuator. IEEE Trans Control Syst Technol 4(3):209–216

Humphris ADL, Miles MJ, Hobbs JK (2005) A mechanical microscope: high-speed atomic force microscopy. Appl Phys Lett 86:034106-1–034106-3

Leang KK, Devasia S (2007) Feedback-linearized inverse feedforward for creep, hysteresis, and vibration compensation in afm piezoactuators. IEEE Trans Control Syst Technol 15(5):927–935

Leang KK, Zou Q, Devasia S (2009) Feedforward control of piezoactuators in atomic force microscope systems. Control Syst Mag 29(1):70–82

Meyer E, Hug HJ, Bennewitz R (2004) Scanning probe microscopy. The lab on a tip. Springer, Heidelberg

Newcomb CV, Flinn I (1982) Improving the linearity of piezoelectric ceramic actuators. IEE Electron Lett 18(11):442–443

Picco LM, Bozec L, Ulcinas A, Engledew DJ, Antognozzi M, Horton M, Miles MJ (2007) Breaking the speed limit with atomic force microscopy. Nanotechnology 18(4):0440301–0440304

Rost MJ, Crama L, Schakel P, van Tol E, van Velzen-Williams GBEM, Overgauw CF, ter Horst H, Dekker H, Okhuijsen B, Seynen M, Vijftigschild A, Han P, Katan AJ, Schoots K, Schumm R, van Loo W, Oosterkamp TH, Frenken JWM (2005) Scanning probe microscopes go video rate and beyond. Rev Sci Instrum 76(5):053710-1–053710-9

Yi KA, Veillette RJ (2005) A charge controller for linear operation of a piezoelectric stack actuator. IEEE Trans Control Syst Technol 13(4):517–526